Genes & Diseases (2020) 7, 636–648

Available online at www.sciencedirect.com

ScienceDirect

journal homepage: http://ees.elsevier.com/gendis/default.asp

FULL LENGTH ARTICLE

Adenomyosis-derived extracellular vesicles endow endometrial epithelial cells with an invasive phenotype through epithelial-mesenchymal transition

Dayong Chen, Hai Qiao, Yiting Wang, Ling Zhou, Na Yin, Liaoqiong Fang **, Zhibiao Wang*

State Key Laboratory of Ultrasound Engineering in Medicine Co-Founded by Chongqing and the Ministry of Science and Technology, College of Biomedical Engineering, Chongqing Key Laboratory of Biomedical Engineering; Chongqing Medical University, 40016, PR China

Received 16 September 2019; received in revised form 12 January 2020; accepted 15 January 2020
Available online 23 January 2020

KEYWORDS
Adenomyosis;
Epithelial-mesenchymal transition;
Extracellular vesicles;
Primary endometrial epithelial cells;
Pathogenesis

Abstract Extracellular vesicles from highly metastatic tumor cells have been shown to mediate epithelial-mesenchymal transition (EMT)-related events in recipient cells. In endometrial epithelial cells, EMT processes are known to be involved in the development of adenomyosis. We aimed to investigate whether adenomyosis-derived extracellular vesicles (AMEVs) are able to induce an EMT process in endometrial epithelial cells. In this study, AMEVs were isolated from patients with adenomyosis and characterized by transmission electron microscopy, Western blot, and nanoparticle tracking. Primary endometrial epithelial cells (EECs) were derived from normal endometrium tissues from patients with leiomyoma and co-cultured with AMEVs *in vitro*. AMEV uptake was examined by fluorescence confocal microscopy. The invasion of EECs was confirmed by Transwell assay. Immunohistochemistry, Western blot, and qRT-PCR were performed on EECs to illustrate the expression levels of cytokeratin 19, E-cadherin, vimentin, and zinc finger E-box-binding homeobox 1 (ZEB1). The results indicated that the cellular fluorescence intensity gradually increased after 48 h of co-culture, but decreased after 72 h. After co-culturing with AMEVs for 72 h, EECs expressed significantly lower levels of cytokeratin 19 and E-cadherin, and significantly higher levels of vimentin and ZEB1. Together these results demonstrated that AMEVs

* Corresponding author. State Key Laboratory of Ultrasound Engineering in Medicine Co-Founded by Chongqing and the Ministry of Science and Technology, Chongqing Key Laboratory of Biomedical Engineering, College of Biomedical Engineering, Chongqing Medical University, No.1 Yixueyuan Road, Yuzhong District, Chongqing, 400016, PR China.
** Corresponding author. State Key Laboratory of Ultrasound Engineering in Medicine Co-Founded by Chongqing and the Ministry of Science and Technology, Chongqing Key Laboratory of Biomedical Engineering, College of Biomedical Engineering, Chongqing Medical University, No.1 Yixueyuan Road, Yuzhong District, Chongqing, 400016, PR China.
E-mail addresses: lqfang06@163.com (L. Fang), wangzb@cqmu.edu.cn (Z. Wang).
Peer review under responsibility of Chongqing Medical University.

https://doi.org/10.1016/j.gendis.2020.01.011

induce an EMT process and enhance the invasion of EECs. These changes may contribute to the pathogenesis and progression of adenomyosis.

Introduction

Adenomyosis is a gynecologic medical condition characterized by the abnormal invasion of endometrial epithelial cells (EECs) and stromal cells deep into the myometrium,[1] and it threatens the uterine health of women all over the world. While the pathogenesis of adenomyosis remains unclear, its development may be explained by acquired invasiveness of endometrial cells. Previous studies have implicated the epithelial-mesenchymal transition (EMT) in disease progression.[2]

Through the process of EMT, epithelial cells first lose their polarity and intercellular adhesion, then acquire the ability to migrate, and finally convert to a mesenchymal phenotype.[3] This transition is essential for development and wound healing, as well as for cancer metastasis. Loss of E-cadherin is considered to be a critical event during EMT, involving certain transcription factors such as ZEB1, which could affect the expression of both epithelial (e.g., E-cadherin) and mesenchymal (e.g., N-cadherin, vimentin) markers.[4] Previous reports have described the invasive behavior of EECs during ectopic endometrial implantation.[5–7] EMT processes of EECs were postulated to play a pivotal role in the progression of adenomyosis.

Recent studies have demonstrated the involvement of extracellular vesicles (EVs) in EMT-associated events, inducing the formation of pre-metastatic niches.[8] In addition to their apparent role in EMT, EVs are also known to be involved in cell—cell communication, homeostasis, and disease progression.[9–11] EVs, including microvesicles and exosomes, are lipid bilayer-delimited particles derived from various cell types; they have been isolated from human uterus, uterine epithelial cells, and endometriotic stromal cells.[12,13] Notably, EVs isolated from several different cell models have been observed to induce EMT in recipient cells.[14,15]

In the present study, adenomyosis-derived EVs (AMEVs) were isolated from adenomyotic lesions, EECs were collected from normal endometrium tissues, and then they were co-cultured *in vitro* (Fig. 1). The expression levels of E-cadherin, cytokeratin 19, vimentin, and ZEB1 were detected in order to understand the possible effect of AMEVs on the invasion and EMT process of EECs. The results might provide a new insight for exploring the recurrence and progression of adenomyosis.

Materials and methods

Ethical approval

The study of human tissue specimens as performed in these experiments was approved by the Ethical Committee of Chongqing Medical University. Each patient provided written informed consent. Reference Number:2018014.

Patients and samples collection

This study was conducted on 30 Chinese women, 18 of whom were diagnosed with adenomyosis (9 proliferate, 9 secretory) and 12 with leiomyoma (6 proliferate, 6 secretory) by transvaginal ultrasound, and who were all undergoing hysterectomy at the First Affiliated Hospital of Chongqing Medical University (see Table S1). None of the women had received any hormonal therapies for at least 3 months before hysterectomy. All tissue samples were evaluated by two gynecological pathologists to confirm tissue quality. The study was conducted in accordance with the Declaration of Helsinki of the World Medical Association. Clinical history of patients was obtained as published previously.[16]

Isolation and identification of AMEVs

AMEVs were isolated and purified using previously published protocols.[11] Briefly, fresh adenomyotic lesions were washed in cold phosphate-buffered saline (PBS) (Hyclone, USA) and immediately homogenized. Differential centrifugation was used to remove tissue debris and red blood cells from the homogenates (800×*g* for 10 min followed by 1000×*g* for 10 min), which were then ultrafiltered through a 1.2 μm Minisart Syringe Filter (Sartorius, Germany). The supernatant was then subjected to differential centrifugation (50,000×*g* for 90 min followed by 100,000×*g* for 90 min) and the resulting pellet resuspended in 1 mL PBS. The retained precipitates were further purified by layering them onto iodixanol (AXIS-SHIELD, Norway) density medium with a top-down gradient of 5, 10, 20, 30, 40, and 50%, and centrifuging at 100,000×*g* for 90 min. A gradient layer of the density medium containing purified EVs was then collected from the tube side with a 2 mL pipette, and EVs were washed with 3 mL cold PBS and centrifuged at 100,000×*g* for 90 min. Purified EVs were resuspended in PBS and stored at −80 °C. The membrane protein markers of AMEVs were then evaluated by mass spectrometry and Western blot using three commercially available antibodies purchased from Abcam plc, USA: flotillin 2 (1:1000; ab181988, Abcam plc, USA), CD9 (1:2000; ab92726, Abcam plc, USA), and CD63 (1:1000; ab134045, Abcam plc, USA).

High-performance liquid chromatography-mass spectrometry (LC-MS)

All LC-MS analysis was performed on a Q-Exactive mass spectrometer (Thermo Fisher Scientific, USA). Protein

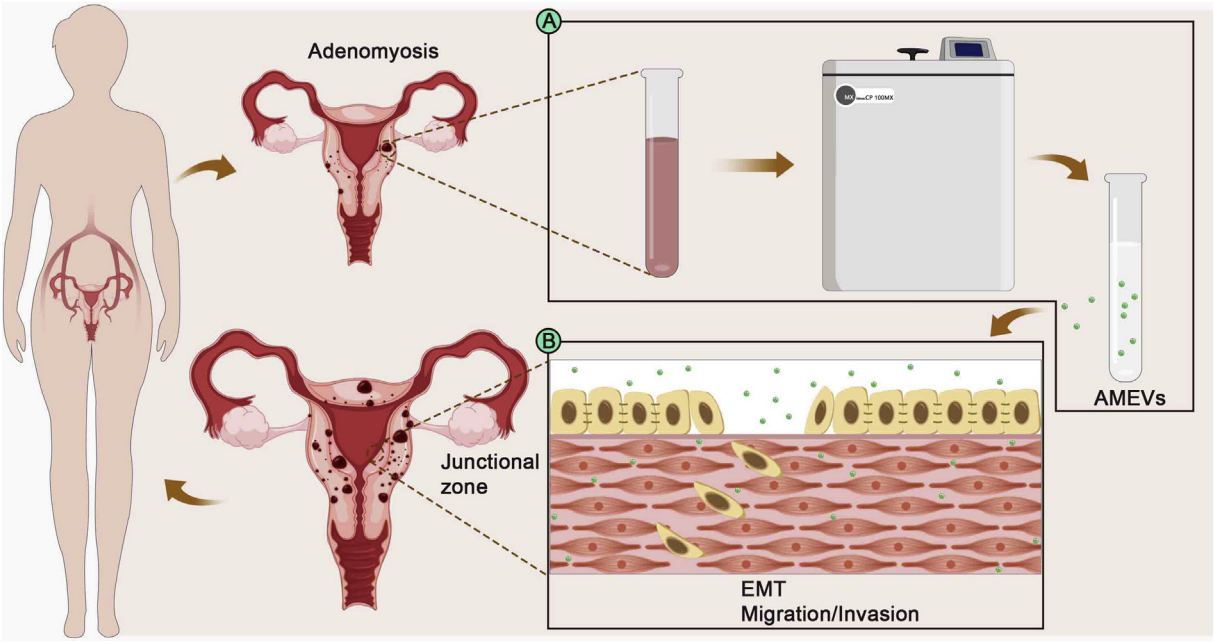

Figure 1 Schematic illustration of the effect of AMEVs on EECs. (A) AMEVs were isolated from adenomyosis tissues. (B) EECs were co-cultured with AMEVs *in vitro*.

identification was performed with MASCOT software by searching Uniprot. Carbamidomethylation of cysteines was set as a fixed modification. The first, overnight, digestion was done with a trypsin-to-protein mass ratio of 1:50, and the second, 4 h, digestion was done at 1:100. The maximal mass tolerance in MS mode was set to 20 ppm for the first search and fragment mass tolerance was set to 0.6 Da. The maximum false discovery rate (FDR) for both peptide and protein identification were set to 0.05.

Isolation and identification of primary endometrial epithelial cells

As described in previous studies,[14,17] endometrial tissues collected from leiomyoma patients were minced and homogenized immediately, then enzymatically digested in 1 mg/mL of collagenase IV (Sigma, USA) with gentle shaking at 37 °C for 60 min. The cells were filtered through a 100 μm cell strainer (Corning, USA) and then a 40 μm cell strainer (Corning, USA) to remove tissue debris. Glandular elements from the 40 μm membrane were backwashed several times with PBS and transferred to a universal tube and pellet by centrifugation at 300×*g* for 5 min. The sediment was then collected and resuspended in Dulbecco's modified Eagle's medium (DMEM) (Hyclone, USA) + 10% fetal bovine serum (FBS) (Hyclone, USA) + 1% penicillin/streptomycin (Beyotime Biotechnology, China) and incubated for 14 days at 37 °C and 5% CO_2. Antibodies purchased from Abcam plc, USA, were used to identify EECs: rabbit anti-cytokeratin 19 (1:200; ab52625, Abcam plc, USA) and goat anti-rabbit IgG - Alexa Fluor® 488 (1:200; ab150077, Abcam plc, USA).

Nanoparticle tracking analysis

Purified AMEVs (1 μL) were diluted in 1 mL PBS and quantified using nanoparticle tracking analysis (Malvern Nanosight NS 3000, UK) to determine the size distribution and particle concentration.

Transmission electron microscopy (TEM) with negative-contrast staining

Purified AMEVs (1 uL) were resuspended in 100 μL PBS, dried onto TEM grids (freshly glow discharged 300 mesh formvar/carbon-coated) (Ted Pella, USA), and negatively stained with 2% Potassium Phosphotungstate. All transmission electron micrographs were obtained using an H7500 transmission electron microscope (Hitachi, Japan) operated at 80 KV.

Low vacuum scanning electron microscopy (LVSEM)

AMEVs (1 uL) were resuspended in 100uL PBS, and then resuspended in 900uL glutaraldehyde solution (2.5%) (P1126, BeiJing Solarbio Science & Technology Co. Ltd, China) at 4 °C overnight. Micrographs of AMEVs were obtained using a low vacuum scanning electron microscopy (Nova Nano SEM 450, FEI, USA) operated at 5 KV.

Laser scanning confocal microscopy (LSCM)

The uptake of AMEVs by EECs was performed as described previously.[18] Briefly, AMEV pellets (30 μL, approximately

$8.04 \times 10^{10} \pm 1.128 \times 10^{10}$ particles) were incubated with a DiO dye (Beyotime Biotechnology, China) solution (10 μM) for 30 min at 37 °C. After washing twice with PBS, pellets were centrifuged at 100,000×*g* for 90 min, and DiO-AMEVs were resuspended in 100 μL of PBS. EECs (1×10^6/mL) were incubated with DAPI dye (Beyotime Biotechnology, China) (10 μg/mL) in a 15 mm glass bottom cell culture dish (NEST, Hong Kong, China) at 37 °C for 24 h, then washed three times with PBS and treated with DMEM containing 10 μL of DiO-AMEVs for 0 h, 48 h, and 72 h. Images were obtained using laser scanning confocal microscopy (Nikon Microsystems, Japan). Digital images were recorded and analyzed using NIS 4.2 Viewer (Nikon Microsystems, Japan).

Fluorescence activated cell sorting (FACS) analysis

To study the effect of inhibiting actin polymerization on AMEV uptake, AMEV pellets (30 μL) were incubated with a DiI dye (Beyotime Biotechnology, China) solution (10 μM) for 30 min at 37 °C. After washing twice with PBS, pellets were centrifuged at 100,000×*g* for 90 min, and DiI-labeled AMEVs were resuspended in 100 μL PBS. EECs (1×10^6/mL) were co-cultured with the actin polymerization inhibitor cytochalasin D (10 μM; C102396, aladdin, China) for 1 h, and then for an additional 6 h with DiI-labelled AMEVs, after which the cultured cells were washed 3 times with PBS. The percentage of fluorescent cells was quantified by FACS analysis (BD Accuri Flow Cytometer) using FlowJo software version 7.6 (TreeStar Inc.).

Cell viability assays

EECs were placed in a 96-well plate at a density of 1×10^4/well. Then, 100 μL of cell culture medium plus 1, 2, 4, 8, 16, 32, 64, or 100 uL of AMEVs was added (6 wells per dose). After 72 h, 10 μL of cell counting kit-8 (CCK-8) solution (Enzo Life Sciences, USA) was added to the cells. Optical density values were obtained at 450 nm using an ELx800 Universal Microplate Reader (Bio-Tek Instruments, USA). All assays were performed three times.

EEC invasion assay

EEC invasion assay was performed as described previously.[19] Briefly, the upper chamber of a 24-well Transwell plate (Corning, USA) was coated with matrigel (R&D Systems, USA) that had been diluted in DMEM (matrigel/DMEM = 1:8). The plates were dried on super-clean bench at 37 °C for 30 min prior to cell seeding. EECs were cultured in serum-free medium for 24 h to starve the cells and then inoculated into 24-well Transwell plates. EECs (200 uL, 1×10^6/mL) in 10% FBS + DMEM medium were seeded into the upper chamber, and 10% FBS + DMEM + 30 μL AMEV solution (approximately $8.04 \times 10^{10} \pm 1.128 \times 10^{10}$ particles/L) was used as a chemoattractant. Cells that migrated to the bottom chamber were fixed in 100% methanol and stained with 0.5% crystal violet. Cell quantification was performed by randomly selecting five regions of the filter and counting the cells in each region. The experiments were repeated three times.

Immunohistochemistry (IHC) and immunocytochemistry (ICC)

Immunochemistry staining procedures were performed as described previously.[20,21] Briefly, expression levels of E-cadherin (1:500; ab40772, Abcam plc, USA), cytokeratin 19 (1:400), vimentin (1:100; AF7013, Affinity Biosciences, USA), ZEB1 (1:100; ab203829, Abcam plc, USA), and HSPB1 (1:100; ab203829, Abcam plc, USA) were determined using specific, commercially available antibodies. Control sections (incubated without the primary antibody) showed little to no immunostaining. Five digital images were collected from random areas of IHC slides using an optical microscope (BX51, Olympus, Japan) and ISCapture software (Tucsen, China). Immunostaining intensity was then quantified using Image Pro Plus v. 6.0 software (Media Cybernetics, USA).

Western blot

Proteins were separated with SDS-PAGE (Beyotime Biotechnology, China) using a 10% separation gel and then transferred to a PVDF (Millipore, USA) membrane. After the transfer, the membrane was blocked with 5% nonfat milk in PBS (pH 7.2) + 0.1% Tween 20 (BeiJing Solarbio Science & Technology Co. Ltd, China). After washing three times with wash buffer (PBS (pH 7.2) + 0.1% Tween 20 (BeiJing Solarbio Science & Technology Co. Ltd, China)), the membrane was incubated overnight at 4 °C with primary antibody. Membranes were washed three times with wash buffer and incubated for 1 h at 37 °C with secondary antibody. Unbound secondary antibodies were removed by washing three times with wash buffer, after which the immunoreactive bands were visualized using ECL detection reagents. Films were scanned using the Azure c400 scanner (Azure Biosystems, USA), and labeled bands were quantified using ImageJ software (NIH, USA). Commercially available antibodies were used: E-cadherin (1:2000), cytokeratin 19 (1:2000), vimentin (1:500), ZEB1 (1:500), HSPB1 (1:1000), GAPDH (1:1000; E021060-03, EarthOx, LLC, USA) and a goat polyclonal secondary antibody (1:1000; E030120-01, EarthOx, LLC, USA).

Quantitative reverse transcription-polymerase chain reaction (qRT-PCR)

TRIZOL reagent (G3013, Servicebio, China) was used to extract total RNA from cultured cells, and 1 μg of RNA was used for cDNA synthesis. The cDNA (100 ng) was added to the real-time PCR mixture containing SYBR Green (04 913 914 001, Roche, Switzerland) and the following primers were used: ZEB1, forward 5′-CTGCAGTCCAAGAACCACCCTTG-3′ and reverse 5′-CCACACTCATGAGGTCTTTTACC-3’; GAPDH (used as an internal control), forward 5′- GGAAGCTTGTCATCAATGGAAATC-3′and reverse 5′-TGATGACCCTTTTGGCTCCC-3’. All reactions were run in triplicate using a StepOnePlus™ real-time PCR system (Applied Biosystems Inc, USA), and relative expression levels were calculated using the comparative cycle threshold (Ct value).[22]

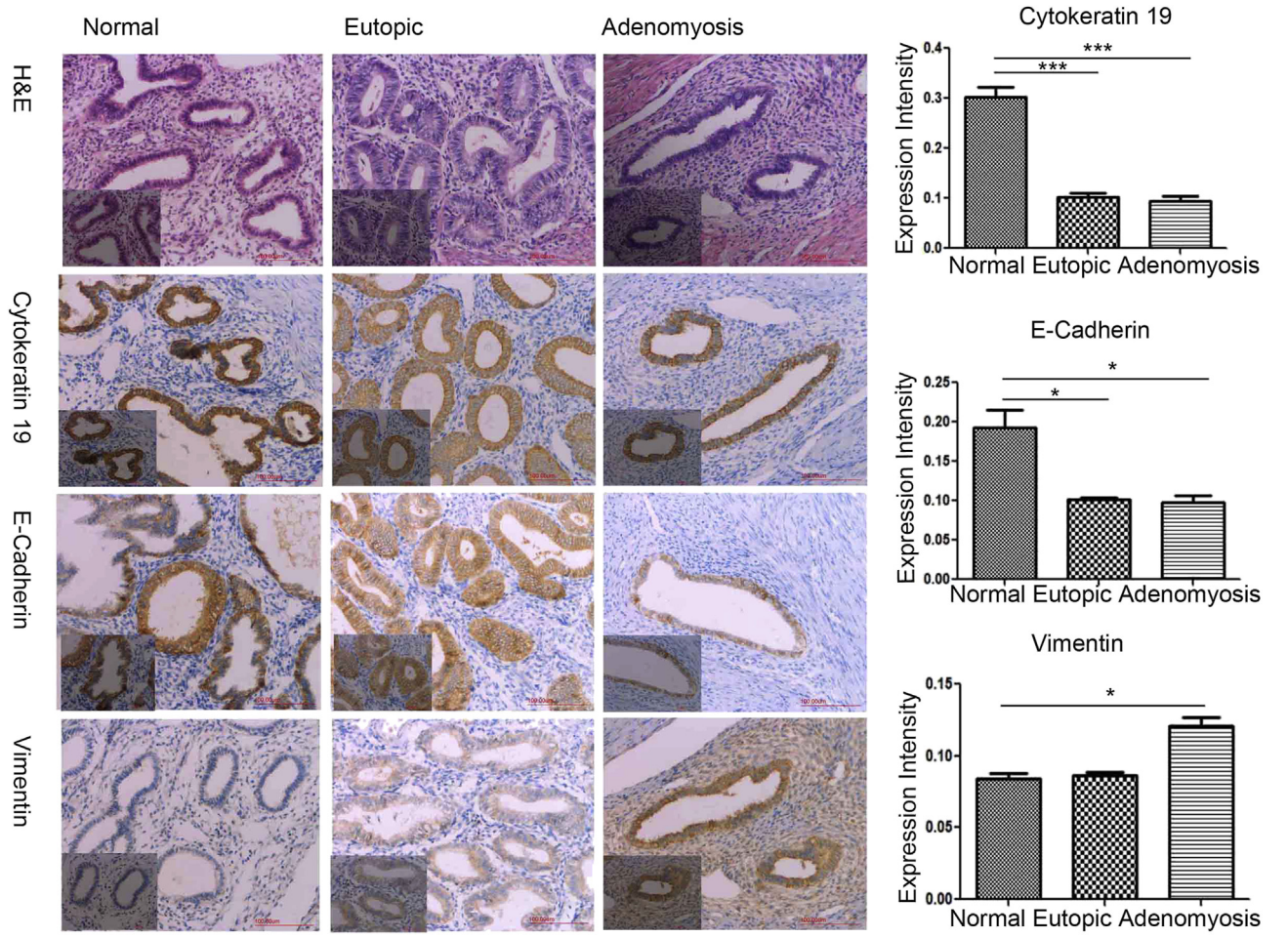

Figure 2 Immunochemistry for EMT markers in normal endometrium, eutopic endometrium, and adenomyosis. The EMT markers cytokeratin 19, E-cadherin, and vimentin were visualized by immunohistochemistry and compared across tissues. Scale bar: 200 μm.

Statistical analysis

All data were analyzed with SPSS software (version 21, IBM, USA) using analysis of variance (ANOVA) or an independent samples t-test. Results are expressed as mean ± standard deviation (SD). The Mann–Whitney U-test was used to compare the incidence of hypermenorrhea in patients with adenomyosis or uterine fibroids. All other categorical variables were expressed as binary and tested by Fisher's exact test; these results are presented as fractions and percentages. For all tests, $P < 0.05$ was considered statistically significant.

Results

EMT occurs in the glandular epithelial cells of adenomyosis samples

To determine whether EMT occurs in adenomyosis, we performed IHC for EMT markers (cytokeratin 19, E-cadherin, and vimentin) in normal (secretory phase, n = 6; proliferate phase, n = 6), eutopic (secretory phase, n = 9; proliferate phase, n = 9), and adenomyotic endometrial tissue (n = 18). Representative IHC results, and the expression profile of EMT markers, are shown in Fig. 2. Cytokeratin 19 and E-cadherin were both present in the majority of normal, eutopic, and adenomyotic tissue, particularly in the cytomembrane and cytoplasm of glandular epithelial cells. Positive vimentin staining was detected in the cytomembrane and cytoplasm of partial glandular epithelial cells and total stromal cells.

In the proliferative phase of normal endometrial epithelial cells, the protein level of cytokeratin 19 was significantly higher than in eutopic endometrium ($P < 0.05$) and adenomyosis lesions ($P < 0.05$) (Fig. 2). In the secretory phase, the level of cytokeratin 19 was significantly higher in the epithelial cells of eutopic endometrium than in control endometrium ($P < 0.05$). A significant decrease in cytokeratin 19 staining was observed in eutopic endometrium and adenomyosis lesions.

E-cadherin expression was lower in eutopic endometrium and adenomyosis lesions than in normal endometrium. Vimentin levels were significantly higher in adenomyotic lesions compared with normal endometrium ($P < 0.05$), but not significantly different between normal and eutopic or eutopic and adenomyotic tissues (Fig. 2).

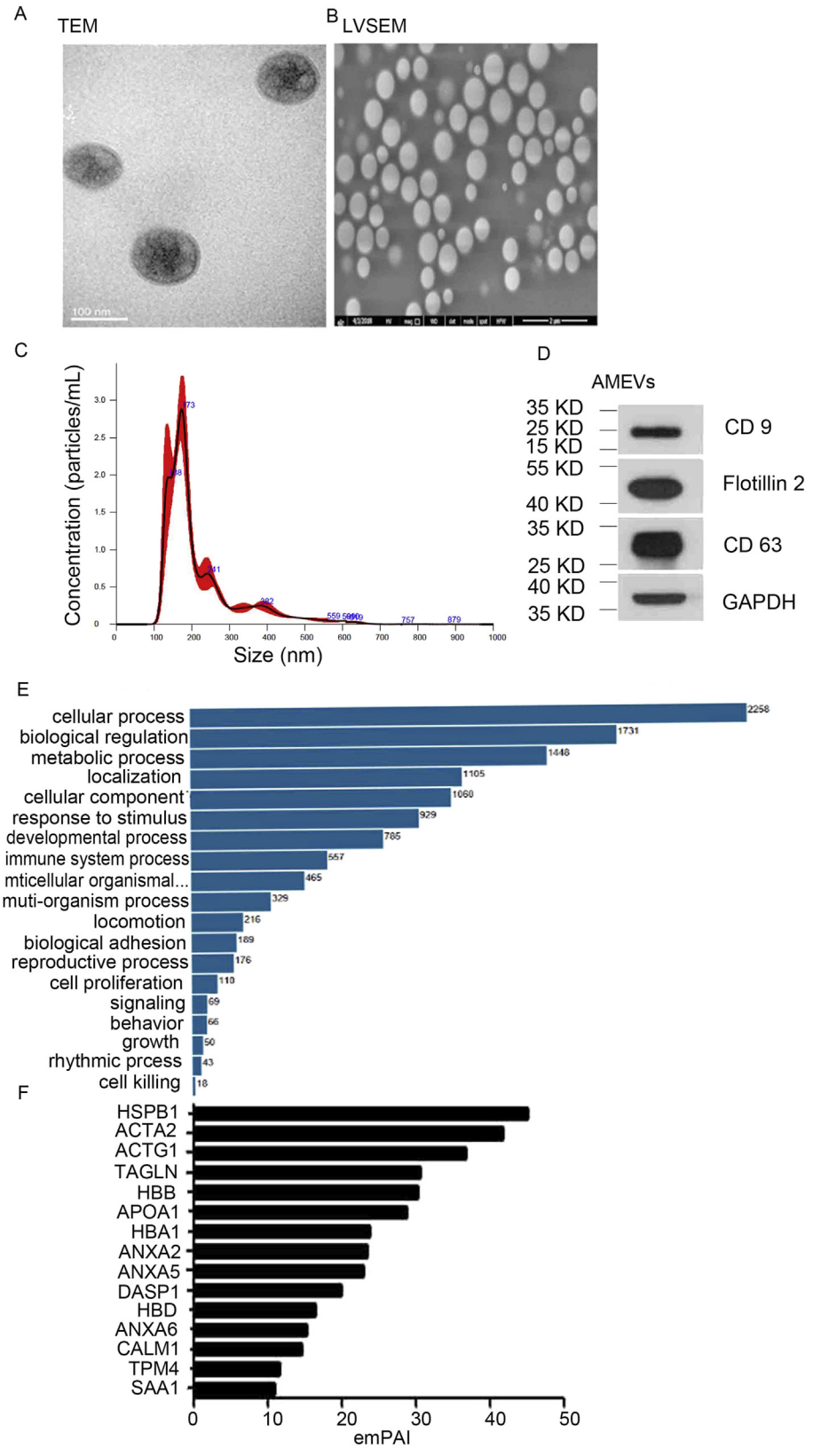

Figure 3 **Biological characteristics of AMEVs.** **(A)** TEM image with negative staining, **(B)** LVSEM image, **(C)** size distribution, and **(D)** membrane biomarker (flotillin-2, CD63 and CD9) of AMEVs. **(E)** Total proteins and **(F)** top 10 proteins enriched in AMEVs.

Table 1 Conventional markers of extracellular vesicles.

Protein family	Accession	Score	Mass	Matches	Sequences	Protein description
Tetraspanins	CD9	223	25,969	20 (9)	6 (3)	CD9 antigen
	CD 63	111	26,474	24 (4)	8 (2)	CD63 antigen
	CD 81	361	26,476	6 (6)	1 (1)	CD81 antigen
Adhersion proteins	CD44	521	82,001	19 (11)	7 (2)	CD44 antigen
	ICAM1	139	58,587	17 (5)	10 (4)	Intercellular adhesion molecule 1
	ITB1	874	91,664	63 (35)	26 (13)	Integrin beta-1
	ITA1	530	132,304	57 (26)	33 (15)	Integrin alpha-1
	ITAV	365	117,048	46 (18)	32 (13)	Integrin alpha-V
	ITAM	409	128,410	40 (16)	31 (12)	Integrin alpha-M
	ITB2	264	87,976	29 (11)	13 (7)	Integrin beta-2
	ITA5	352	115,605	25 (12)	16 (10)	Integrin alpha-5
	ITB3	312	90,194	34 (12)	21 (6)	Integrin beta-3
	ITA6	275	127,724	45 (10)	31 (8)	Integrin alpha-6
	ITB5	148	91,303	41 (6)	14 (5)	Integrin beta-5
	ITA2B	239	114,446	11 (8)	9 (6)	Integrin alpha-IIb
	ITA3	128	117,735	29 (6)	23 (5)	Integrin alpha-3
	ITA11	103	134,527	26 (4)	20 (4)	Integrin alpha-11
	ITA7	91	130,121	20 (3)	16 (3)	Integrin alpha-7
	ITAL	79	129,942	14 (3)	12 (3)	Integrin alpha-L
	ITA2	70	130,468	20 (3)	14 (3)	Integrin alpha-2
	ITA9	28	115,727	17 (1)	15 (1)	Integrin alpha-9
	ITA4	26	116,252	20 (1)	15 (1)	Integrin alpha-4
	ITB4	53	205,745	42 (1)	30 (1)	Integrin beta-4
Vesicle trafficking-related proteins	ANXA1	2530	38,918	115 (79)	31 (19)	Annexin A1
	ANXA2	4829	38,808	207 (156)	40 (27)	Annexin A2
	ANXA3	184	36,524	11 (5)	11 (5)	Annexin A3
	ANXA4	1292	36,088	78 (41)	32 (16)	Annexin A4
	ANXA5	2201	35,971	107 (68)	34 (25)	Annexin A5
	ANXA6	4079	76,168	209 (144)	68 (45)	Annexin A6
	ANXA7	486	52,991	46 (19)	26 (12)	Annexin A7
	ARF3	651	20,645	55 (27)	15 (10)	ADP-ribosylation factor 3
	ARF4	564	20,612	37 (25)	13 (9)	ADP-ribosylation factor 4
	ARF5	486	20,631	40 (20)	15 (7)	ADP-ribosylation factor 5
	ARF6	233	20,183	26 (11)	12 (5)	ADP-ribosylation factor 6
	TSG101	45	44,088	28 (1)	16 (1)	Tumor susceptibility gene 101 protein
Flotillins	FLOT1	357	47,554	45 (11)	26 (8)	Flotillin-1
	FLOT2	478	47,434	39 (17)	21 (11)	Flotillin-2

The structural characteristics and protein cargoes of AMEVs

AMEVs were isolated from adenomyosis lesions (Fig. 3A). TEM with negative contrast staining and LVSEM were used to visualize AMEVs (Fig. 3B). AMEVs were approximately 100—1000 nm in diameter and had a round shape.

Nanoparticle tracking analysis revealed that the AMEVs at 50,000×*g* +100,000×*g* had a mean diameter of 221.0 ± 8.3 nm and mean concentration of $2.68 \times 10^{12} \pm 3.76 \times 10^{11}$ particles/ml (Fig. 3C).

LC-MS revealed notable enrichment in AMEVs for conventional EV markers,[23] including tetraspanins, adhesion proteins, vesicle trafficking-related proteins, and flotillins (Table 1).

Therefore, we used Western blotting to determine expression levels of flotillin-2, CD9, and CD63 as markers of AMEVs (Fig. 3D).

In total, 2449 proteins were found to be involved in the cell biological process (Fig. 3E). The top 10 enriched proteins (with an exponentially modified protein abundance index (emPAI) > 10) in AMEVs included: annexin A2, annexin A5, annexin A6, HSPB1, and Transgelin (Fig. 3F) (Table S2).

Cellular uptake, intracellular distribution, and invasive changes of EECs

To investigate the effect of AMEVs on EECs, EECs were isolated from normal endometrium. Immunocytochemistry and immunofluorescence staining showed that cytokeratin 19 was expressed in EECs, and that the purity of EECs was up to 95% (Fig. S1).

When co-cultured with DiO-labeled AMEVs for 0 h, 48 h, and 72 h, LSCM showed that the cellular fluorescence intensity of EECs was slightly higher at 48 h, but not at 72 h,

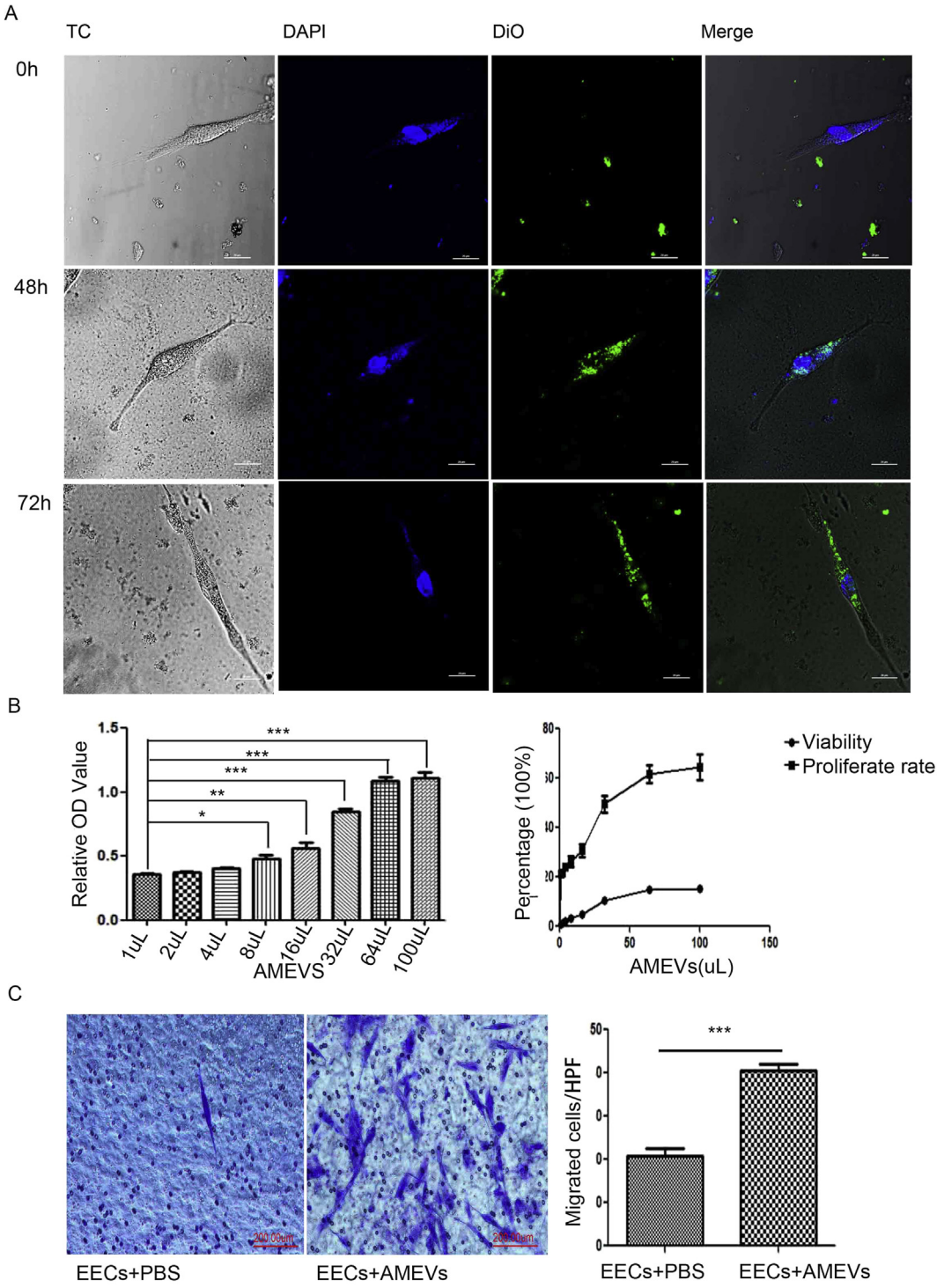

Figure 4 Cellular endocytosis and distribution, and invasive changes of EECs. (A) Confocal microscopy images of the endocytosis of DiO-labeled AMEVs (green fluorescence) in EECs for 0, 48, and 72 h. After coculture with AMEVs for 72 h, the cell viability and proliferation rate **(B)** and invasive ability **(C)** of EECs were enhanced ($n = 6$ per group; $P < 0.05$ for all). Scale bar: 200 μm. The asterisk indicates a comparison made to the control. $^{*}P < 0.05$; $^{**}P \leq 0.01$; $^{***}P \leq 0.001$ for all figures.

as compared to baseline. The AMEVs were typically concentrated in the cytoplasm, particularly in the subcellular compartment (Fig. 4A).

To further examine the toxicity of AMEV to EEC, we evaluated the effect of AMEV on cell viability and cell proliferation using CCK-8. After co-culturing with 8 μL of AMEVs for 72 h, both EEC viability and proliferation were significantly increased compared to untreated controls ($n = 6$, $P < 0.05$). This effect was even more pronounced when EECs were treated with 30 μL of AMEVs (Fig. 4B).

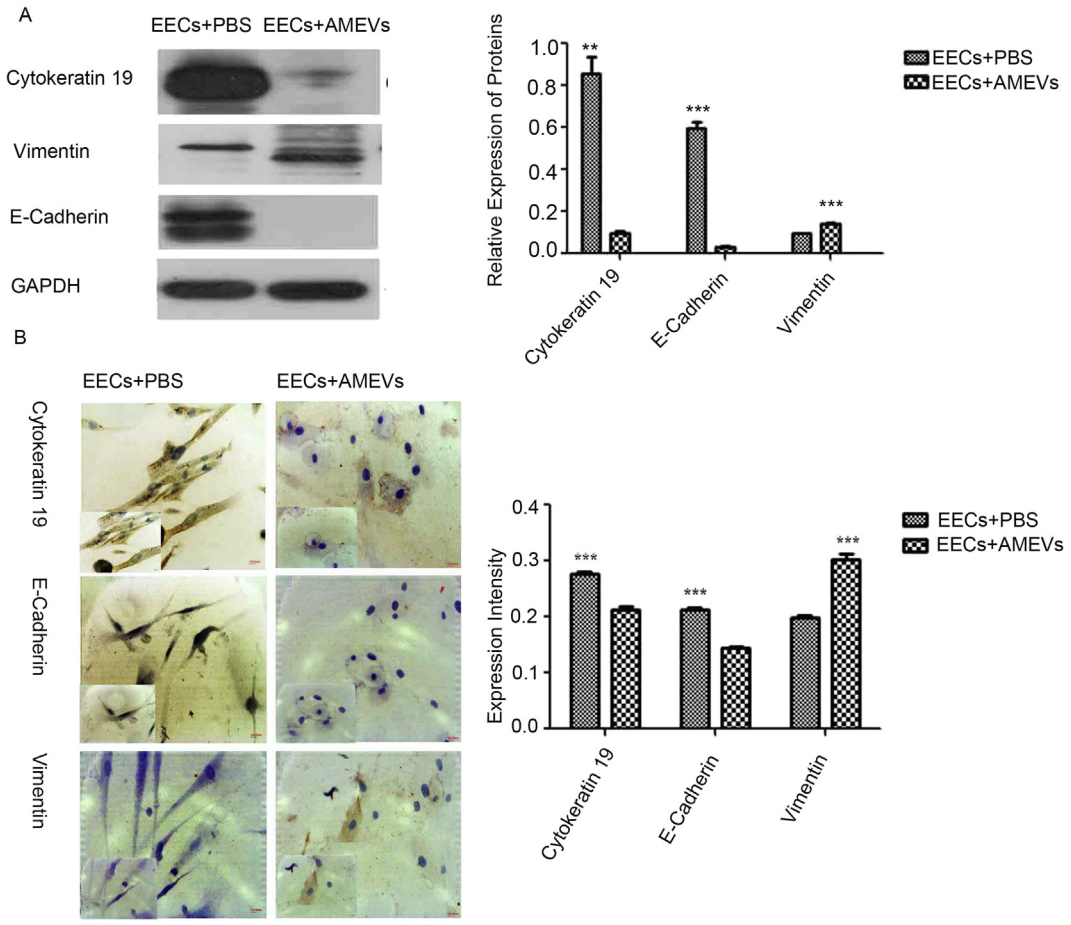

Figure 5 An EMT-like process in EECs induced by AMEVs. When cocultured with AMEV for 72 h, Western Blot **(A)** and immunochemical staining **(B)** showed that cytokeratin 19 and E-cadherin expression was significantly decreased, and vimentin increased, as compared to the control group ($P < 0.05$). Scale bar: 200 μm.

Based on the Transwell assay, 72 h of co-culture with AMEVs appeared to promote migration and invasion of EECs ($n = 6$, $P < 0.05$) (Fig. 4C).

An EMT-like process in EECs induced by AMEVs

During EMT, cells lose E-cadherin expression, intermediate filaments switch from cytokeratin to vimentin, and vimentin expression is increased.[24,25] Therefore, after being treated with AMEVs for 72 h, Western blot showed that EEC lysates expressed significantly less cytokeratin 19 ($n = 3$, $P < 0.05$) and E-cadherin ($n = 3$, $P < 0.05$), and significantly more vimentin ($n = 3$, $P < 0.05$), than untreated controls (Fig. 5A).

To further confirm these changes, immunocytochemistry also demonstrated that levels of cytokeratin 19 and E-cadherin were significantly lower in treated than in untreated EECs ($n = 3$, $P < 0.05$), and levels of vimentin were significantly higher ($n = 3$, $P < 0.05$) (Fig. 5B).

HSPB1 and ZEB1 expression during EMT

To identify EMT-related proteins, LC-MS combined with the Uniprot database revealed 20 EMT-related proteins in AMEVs (Fig. 6A, Table 2). Of these proteins, HSPB1 and Annexin A2 had an emPAI>20, HSPA5 and MSN had an emPAI>5, S100A4 and EZR had an emPAI≥1, and 14 proteins had an emPAI<1 (CTBP1, CTNNB1, PDCD6, PPP3R1, PEF1, CTBP2, TRIM28, RTN4, DDX17, CCAR2, GSK3B, PDCD4, BMP7, and ENG). HSPB1 had the highest emPAI (44.96), and Annexin A2 ranked eighth (23.25).

To analyze the network clustering of these 20 EMT-related proteins, the STRING Database (version 11.0) (https://string-db.org/) showed that HSPB1 could interact with HSPA5, MSN, and CTNNB1. Immunohistochemical staining showed that HSPB1 expression was significantly increased after co-culture with AMEVs ($P < 0.05$) (Fig. 6B). FACS analysis revealed that EEC uptake of AMEVs was significantly inhibited by cytochalasin D ($P < 0.05$) (Fig. 6C), and HSPB1 expression was significantly reduced after co-culture with AMEVs and cytochalasin D ($P < 0.05$) (Fig. 6D).

The E-cadherin transcriptional repressor ZEB1 was not expressed in AMEVs. To examine whether AMEVs enhance the mRNA and protein level of ZEB1 during EMT in EECs, immunochemical staining and qRT-PCR were used to examine the mRNA and protein level of ZEB1 in EECs. After co-culturing EECs with AMEVs for 72 h, immunochemical staining showed that ZEB1 expression was significantly higher in treated EECs than in untreated controls ($n = 3$, $P < 0.05$) (Fig. 6E).

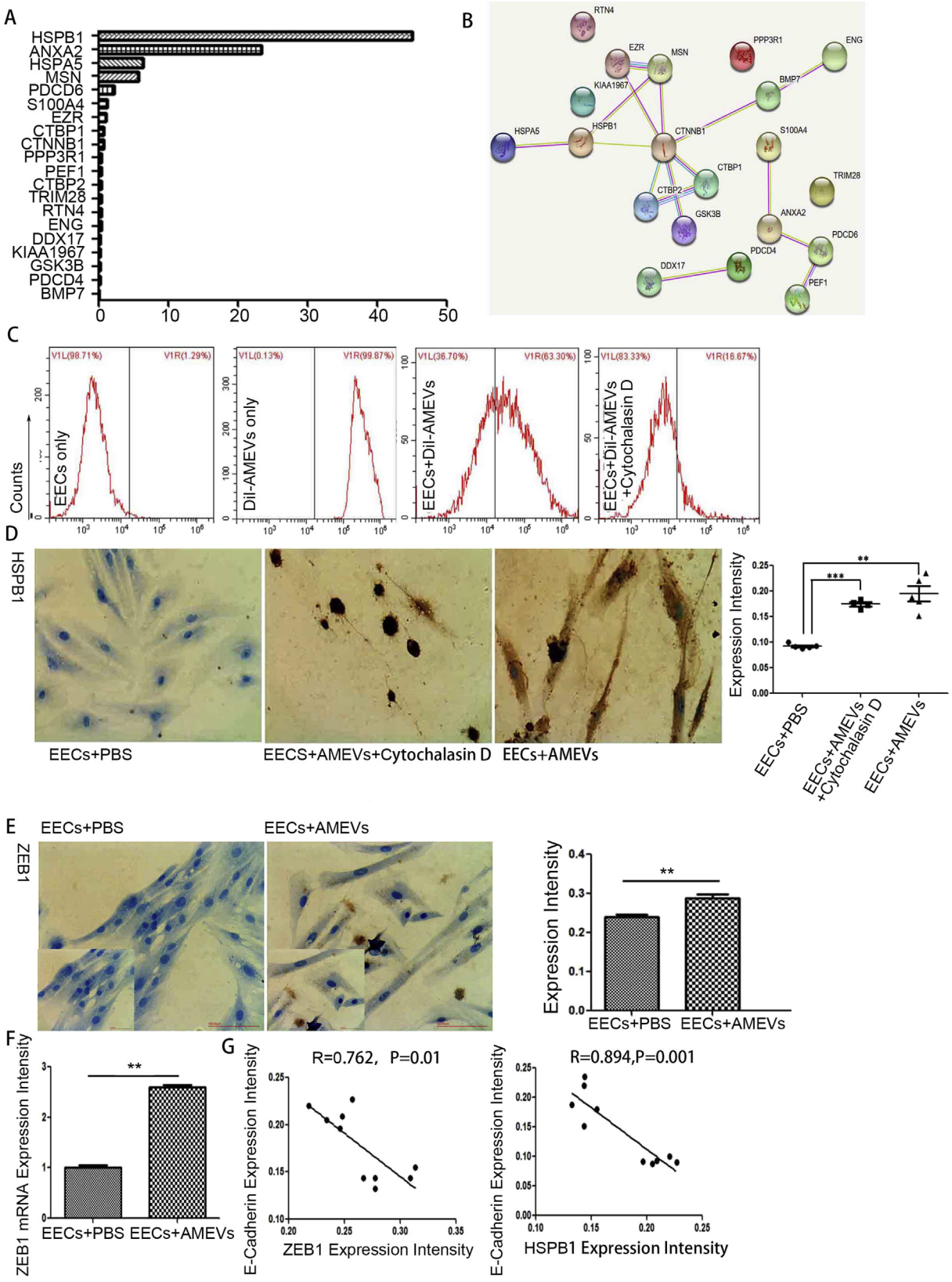

Figure 6 HSPB1 and ZEB1 expression during EMT of EECs. (A) EMT-related proteins and **(B)** network clustering of EMT-related proteins in AMEVs. **(C)** Effect of cytochalasin D on endocytosis of AMEVs and **(D)** HSPB1 expression in EECs treated with AMEVs for 72 h. After 72 h co-culture with AMEVs, immunochemical staining ($P < 0.05$) **(E)** and qRT-PCR ($P < 0.05$) **(F)** showed that ZEB1 expression in EECs was up-regulated, and E-cadherin expression levels were negatively correlated with ZEB1 ($R = 0.762$, $P < 0.05$) and HSPB1 ($R = 0.894$, $P < 0.05$) expression levels **(G)**. Scale bar: 100 μm.

Table 2 20 EMT-related proteins in AMEVs.

Protein name	Gene name	Score	Mass	Matches	Sequences	emPAI
Heat shock protein beta-1	HSPB1 HSP27 HSP28	2829	22,826	142 (104)	20 (17)	44.96
Annexin A2	ANXA2 ANX2 ANX2L4 CAL1H LPC2D	4829	38,808	207 (156)	40 (27)	23.25
78 kDa glucose-regulated protein	HSPA5 GRP78	3713	72,402	162 (112)	55 (35)	6.36
Moesin (Membrane-organizing extension spike protein)	MSN	1301	67,892	137 (60)	69 (32)	5.61
Programmed cell death protein 6	PDCD6 ALG2	239	21,912	23 (16)	8 (6)	2.13
Protein S100-A4	S100A4 CAPL MTS1	62	11,949	13 (4)	7 (3)	1.13
Ezrin	EZR VIL2	448	69,484	75 (24)	44 (12)	1
C-terminal-binding protein 1	CTBP1 CTBP	223	47,962	26 (11)	14 (8)	0.7
Catenin beta-1	CTNNB1 CTNNB OK/SW-cl.35 PRO2286	362	86,069	34 (16)	22 (13)	0.69
Calcineurin subunit B type 1	PPP3R1 CNA2 CNB	74	19,402	3 (2)	3 (2)	0.38
Peflin	PEF1 ABP32 UNQ1845/PRO3573	110	30,646	7 (4)	5 (3)	0.36
C-terminal-binding protein 2	CTBP2	149	49,427	18 (4)	13 (3)	0.29
Transcription intermediary factor 1-beta	TRIM28 KAP1 RNF96 TIF1B	175	90,261	22 (8)	18 (7)	0.28
Reticulon-4	RTN4 KIAA0886 NOGO My043 SP1507	317	130,250	43 (14)	21 (7)	0.25
Endoglin	ENG END	422	71,559	17 (11)	8 (5)	0.25
Probable ATP-dependent RNA helicase DDX17	DDX17	160	80,906	37 (8)	18 (5)	0.22
Cell cycle and apoptosis regulator protein 2	CCAR2 DBC1 KIAA1967	98	103,465	36 (5)	17 (5)	0.17
Glycogen synthase kinase-3 beta	GSK3B	30	47,228	10 (3)	8 (2)	0.14
Programmed cell death protein 4	PDCD4 H731	63	52,102	17 (2)	12 (2)	0.13
Bone morphogenetic protein 7	BMP7 OP1	26	49,681	7 (1)	7 (1)	0.07

Similarly, qRT-PCR showed that mRNA levels of ZEB1 were significantly higher in treated EECs than in untreated controls ($n = 3$, $P < 0.05$) (Fig. 6F). After treatment with AMEVs, the expression of E-cadherin in EECs was negatively correlated with ZEB1 expression ($R = 0.762$, $P < 0.05$) and HSPB1expression ($R = 0.894$, $P < 0.05$) (Fig. 6G).

Discussion

EVs represent a novel cell communication mechanism that is able to operate over both short and long distances.[25] EVs are shed by both prokaryotic and eukaryotic cells and contain messages for the surrounding biological environment, including exosomes (30—150 nm) and microvesicles (100—1500 nm).[26] In this study, we isolated AMEVs from the homogenate of adenomyotic lesions, and subsequent analysis with LC-MS and western blot showed that AMEVs express conventional markers of exosomes and microvesicles. We did not separate exosomes from microvesicles, because no straightforward criteria exist to distinguish, isolate, and identify subpopulations of cell-derived vesicles. This may be a topic for future study.

EV-mediated cell—cell communication is based on the release and uptake of EVs.[27] Our findings show that AMEVs enhance the viability and proliferation rate of EECs, and the internalization process of AMEVs into EECs increases with time and occurs mainly in the subcellular compartment of the cytoplasm.[28] The process can be inhibited by inhibiting actin polymerization with cytochalasin D.

EVs can transmit intracellular signals, induce EMT, promote tumorigenesis and metastasis, and are important mediators in the tumor microenvironment.[29] In our study, after being co-cultured with AMEVs for 72 h, EECs exhibited enhanced invasiveness, reduced expression of E-cadherin and cytokeratin 19, and increased expression of vimentin and ZEB1. Moreover, the downregulation of E-cadherin was negatively associated with the upregulation of ZEB1. ZEB1 is an E-cadherin transcriptional repressor that binds to the E-cadherin promoter at E-boxes and represses E-cadherin transcription.[30] LC-MS showed that ZEB1 was not expressed in AMEVs. Together these results demonstrate that EMT occurs in EECs after co-culture with AMEVs.[4] As EMT of EECs has been shown to be involved in the pathology of adenomyosis,[6,7] these findings provide insight to better understand the role of AMEVs in etiology and pathophysiology. Therefore, the pathogenesis of adenomyosis may be divided into two stages:

1) EECs acquire high invasiveness through EMT, and highly invasive EECs can easily pass through the basalis of endometrium into myometrium. These changes may be related to high estrogen levels.[7]
2) EVs from existing adenomyotic lesions stimulate EECs to acquire high invasiveness through EMT, promoting the recurrence and progression of adenomyosis.

LC-MS analysis revealed 20 EMT-related proteins in AMEVs, of which HSPB1 had the highest emPAI (44.96). HSPB1 is known to be involved in chaperone activity,

apoptosis, and cellular development and differentiation. HSPB1 has been reported to be associated with EMT in salivary adenoid cystic carcinoma[31] and prostate cancer.[32,33] When EECs were co-cultured with AMEVs for 72 h, our findings showed that HSPB1 expression in EECs was upregulated; in contrast, co-culture with cytochalasin D resulted in down-regulated HSPB1 expression. After co-culture with AMEVs, the downregulation of E-cadherin in EECs was correlated with the upregulation of HSPB1. These results suggest that HSPB1 may participate in the development and progression of adenomyosis.

In conclusion, our findings show that EVs from adenomyotic lesions induce an EMT-like process in EECs and endow EECs with an invasive phenotype. ZEB1 and HSPB1 may be involved in this process. The present findings provide novel insights for exploring the etiology and pathogenesis of adenomyosis and provide great insights into the development of new therapeutic approaches.

Authors' contributions

ZBW, LQF and DYC conceived and designed the study; DYC performed the experiments with the assistance of HQ, YTW and LZ for in vivo work. DYC and LZ analyzed data; DYC and LQF wrote the paper, and all the other authors were involved in writing the manuscript. The samples of adenomyosis, eutopic endometrium and normal endometrium were collected by DYC and NY. All authors edited and approved the final draft of the manuscript.

Funding

This work was partially supported by the National Natural Science Fund by the Chinese National Science Foundation (No.81127901, No.31571453 and No.11604034) and the National Basic Research Program of China (No.2011CB707900 and No.20170412), and the Chongqing Basic Science and Frontier Technology Research Project (No. cstc2017jcyjAX0432), and the Chongqing Postdoctoral Scientific Research Project (No.Xm2017084).

Conflict of interests

The authors declare no conflict of interests.

Acknowledgements

We thank professor JunYing Tang in the Department of Gynecology at the First Affiliated Hospital of Chongqing Medical University for the specimen collection of this scientific research. The authors are grateful to Medjaden Bioscience Limited for their assistance with language editing.

Appendix A. Supplementary data

Supplementary data to this article can be found online at https://doi.org/10.1016/j.gendis.2020.01.011.

References

1. Benagiano G, Habiba M, Brosens I. The pathophysiology of uterine adenomyosis: an update. *Fertil Steril*. 2012;98(3):572—579.
2. Bilyk O, Coatham M, Jewer M, Postovit LM. Epithelial-to-Mesenchymal transition in the female reproductive tract: from normal functioning to disease pathology. *Front Oncol*. 2017;7:145.
3. Acloque H, Adams MS, Fishwick K, Bronner-Fraser M, Nieto MA. EMTs: the importance of changing cell state in development and disease. *J Clin Invest*. 2009;119(6):1438—1449.
4. Thiery JP. Epithelial-mesenchymal transitions in tumor progression. *Nat Rev Canc*. 2002;2(6):442—454.
5. Zeitvogel A, Baumann R, Starzinski-Powitz A. Identification of an invasive, N-Cadherin-Expressing epithelial cell type in endometriosis using a new cell culture model. *Am J Pathol*. 2001;159(5):1839—1852.
6. Oh SJ, Shin JH, Kim TH, et al. beta-Catenin activation contributes to the pathogenesis of adenomyosis through epithelial-mesenchymal transition. *J Pathol*. 2013;231(2):210—222.
7. Chen YJ, Li HY, Huang CH, et al. Oestrogen-induced epithelial-mesenchymal transition of endometrial epithelial cells contributes to the development of adenomyosis. *J Pathol*. 2010;222(3):261—270.
8. Gopal SK, Greening DW, Rai A, et al. Extracellular vesicles: their role in cancer biology and epithelial-mesenchymal transition. *Biochem J*. 2017;474(1):21—45.
9. Ogorevc E, Kralj-Iglic V, Veranic P. The role of extracellular vesicles in phenotypic cancer transformation. *Radiol Oncol*. 2013;47(3):197—205.
10. Mo YM, Siljander P, Andreu Z, et al. Biological properties of extracellular vesicles and their physiological functions. *J Extracell Vesicles*. 2015;4:27066.
11. Coumans FAW, Brisso AR, Buzas EI, et al. Methodological guidelines to study extracellular vesicles. *Circ Res*. 2017;120(10):1632—1648.
12. Racicot K, Schmitt A, Ott T. The myxovirus-resistance protein, MX1, is a component of exosomes secreted by uterine epithelial cells. *Am J Reprod Immunol*. 2012;67(6):498—505.
13. Harp D, Driss A, Mehrabi S, et al. Exosomes derived from endometriotic stromal cells have enhanced angiogenic effects in vitro. *Cell Tissue Res*. 2016;365(1):187—196.
14. Greening DW, Gopal SK, Mathias RA, et al. Emerging roles of exosomes during epithelial-mesenchymal transition and cancer progression. *Semin Cell Dev Biol*. 2015;40:60—71.
15. Kim J, Kim TY, Lee MS, Mun JY, Ihm C, Kim SA. Exosome cargo reflects TGF-beta1-mediated epithelial-to-mesenchymal transition (EMT) status in A549 human lung adenocarcinoma cells. *Biochem Biophys Res Commun*. 2016;478(2):643—648.
16. Shao RY, Xing RX, Xiong Y, Fang LQ, Wang ZB. Differential expression of estrogen receptor a and b isoforms in muLtiple and solitary leiomyomas. *Biochem Biophys Res Commun*. 2015;468(1—2):136.
17. An M, Li D, Yuan M, L QJ, Zhang L, Wang GY. Interaction of macrophages and endometrial cells induces epithelial-mesenchymal transition-like processes in adenomyosis. *Biol Reprod*. 2017;96(1):46—57.
18. Holder B, Jones T, Sancho Shimizu V, et al. Macrophage exosomes induce placental inflammatory cytokines a novel mode of maternal placental. *Traffic*. 2016;17(2):168—178.
19. Korpal M, Lee ES, Hu G, Kang Y. The miR-200 family inhibits epithelial-mesenchymal transition and cancer cell migration by direct targeting of E-cadherin transcriptional repressors ZEB1 and ZEB2. *J Biol Chem*. 2008;283(22):14910—14914.
20. Chen YJ, Yuan CC, Chow KC, et al. Overexpression of dihydrodiol dehydrogenase is associated with cisplatin-based

chemotherapy resistance in ovarian cancer patients. *Gynecol Oncol*. 2005;97(1):110—117.
21. Yang MH, Chiang WC, Chou TY, et al. Increased NBS1 expression is a marker of aggressive head and neck cancer and overexpression of NBS1 contributes to transformation. *Clin Canc Res*. 2006;12(2):507—515.
22. Wang DJ, Wang CMY, Wang YT, Qiao H, Fang LQ, Wang ZB. Lactation-related MicroRNA expression in microvesicles of human umbilical cord blood. *Med Sci Mon Int Med J Exp Clin Res*. 2016;22:4542—4554.
23. Zhang H, Freitas D, Kim HS, et al. Identification of distinct nanoparticles and subsets of extracellular vesicles by asymmetric flow field-flow fractionation. *Nat Cell Biol*. 2018;20(3):332—343.
24. Gavert N, Ben-Ze'ev A. Epithelial-mesenchymal transition and the invasive potential of tumors. *Trends Mol Med*. 2008;14(5):199—209.
25. D'Souza-Schorey C, Clancy JW. Tumor-derived microvesicles: shedding light on novel microenvironment moduLators and prospective cancer biomarkers. *Genes Dev*. 2012;26(12):1287—1299.
26. Nguyen HP, Simpson RJ, Salamonsen LA, Greening DW. Extracellular vesicles in the intrauterine environment: challenges and potential functions. *Biol Reprod*. 2016;95:109.
27. Vader P, Breakefield XO, Wood MJ. Extracellular vesicles: emerging targets for cancer therapy. *Trends Mol Med*. 2014;20(7):385—393.
28. Puzar Dominkus P, Stenovec M, Sitar S, et al. PKH26 labeling of extracellular vesicles: characterization and cellular internalization of contaminating PKH26 nanoparticles. *Biochim Biophys Acta Biomembr*. 2018;1860:1350—1361.
29. Tsai JH, Yang J. Epithelial-mesenchymal plasticity in carcinoma metastasis. *Genes Dev*. 2013;27:2192—2220.
30. Lamouille S, Xu J, Derynck R. Molecular mechanisms of epithelial-mesenchymal transition. *Nature*. 2014;(15):189—196.
31. Chen W, Ren X, Wu J, et al. HSP27 associates with epithelial-mesenchymal transition, stemness and radioresistance of salivary adenoid cystic carcinoma. *J Cell Mol Med*. 2018;22(4):2283—2298.
32. Shiota M, Bishop JL, Nip KM, et al. Hsp27 regulates epithelial mesenchymal transition, metastasis, and circulating tumor cells in prostate cancer. *Canc Res*. 2013;73(10):3109—3119.
33. Cordonnier T, Bishop JL, Shiota M, et al. C Hsp27 regulates EGF/β-catenin mediated epithelial to mesenchymal transition in prostate cancer. *Int J Canc*. 2015;136(6):E496—507.